Dielectric-loaded surface plasmon polariton waveguides: Figures of merit and mode characterization by image and Fourier plane leakage microscopy

J. Grandidier,* S. Massenot, G. Colas des Francs, A. Bouhelier, J.-C. Weeber, L. Markey, and A. Dereux
Institut Carnot de Bourgogne, UMR 5209, CNRS, Université de Bourgogne, 9 Avenue A. Savary, BP 47 870, 21078 Dijon, France

J. Renger, M. U. González, and R. Quidant†
Institut de Ciencies Fotoniques (ICFO), Mediterranean Technology Park, 08860 Castelldefels (Barcelona), Spain
(Received 24 June 2008; revised manuscript received 25 September 2008; published 19 December 2008)

Waveguiding of surface plasmon polaritons by dielectric-loaded metal structures is studied in detail by combining numerical simulations and leakage radiation microscopy. These types of waveguides are first numerically investigated using the effective index model and the differential method. We analyzed systematically the influence of the ridge width and thickness of the waveguide on the properties of the surface plasmon guided modes. In particular we investigated the confinement factor of the modes and their associated propagation lengths. These two parameters can be optimized by adjusting the thickness of the dielectric layer. Waveguides loaded with thick and thin dielectric ridges are then optically characterized by leakage radiation microscopy. The mode propagation distance is measured by direct-space imaging and the propagation constants are evaluated by Fourier imaging and analysis. Good agreements are found between theoretical and experimental data.

DOI: 10.1103/PhysRevB.78.245419 PACS number(s): 73.20.Mf, 71.36.+c, 42.79.Gn, 42.82.Gw

I. INTRODUCTION

Surface plasmon polaritons (SPPs), originating from the coupling of an electromagnetic wave to the free electrons of a metal, open new perspectives in optoelectronics.[1,2] In the last years there has been an increased effort toward the development of surface plasmon-based devices, and the design of appropriate SPP waveguides constitutes a key element in this route. Different configurations have been already proposed and validated, and their degree of applicability analyzed.[2–8]

One of the considered configurations relies on the extension of the concept of dielectric-loaded waveguides to plasmon polariton mode and consists on the deposition of a dielectric stripe atop a metallic surface. This approach has been experimentally demonstrated recently,[9] and the theoretical analysis of the properties of these dielectric-loaded SPP waveguides (DLSPPWs) shows their high potential in integrated photonics.[10,11] In fact, bends, splitters, and couplers based on these DLSPPW have already been experimentally proved.[12,13] Moreover, the dielectric layer can be artificially doped by suitable materials so that its optical properties could be externally modified to actively control the SPP mode. This configuration opens then an interesting way for active plasmonics (e.g., electrically or optically controlled plasmonics).

Taking into account the perspectives offered by this kind of waveguides, a detailed analysis of their performance is needed. This study can be done in terms of appropriate figures of merit defined to describe the suitability of a given configuration to a particular application.[14] In this paper, we provide an extensive study of the dielectric-loaded surface plasmon polaritons waveguides by means of two different figures of merit: one that takes into account the aptness of the DLSPPW to transport information over relatively long distances and the other that evaluates the confinement of the waveguide mode. Based on these figures of merit, we identify two regimes of interest for DLSPPW: thick (thickness $\approx \lambda/2$) and thin (thickness $\ll \lambda/2$) dielectric loads. Thick dielectric loads provide a strong-mode confinement within the dielectric stripe, making them suitable for the development of bends, splitters, and active devices. Thin dielectric loads offer longer propagation distances, allowing their use as simply connecting waveguides.

Once these two regimes have been identified (Sec. II), we have calculated numerically the more appropriate sets of dimensions for each case to highlight their characteristics. These dimensions were used to design and fabricate dielectric structures on thin-metal films. Section III presents the experimental characterization carried out on the fabricated structure to confirm and further analyze their behavior. This experimental study has been done by means of leakage radiation microscopy (LRM).[15–17] LRM is a highly appropriate technique to perform this study since it is possible to image both the direct and Fourier planes. These two operation modes provide information about the intensity distribution and propagation length of the guided modes as well as their effective indices. In a previous letter, we assessed this method by characterizing a rectangular dielectric waveguide used as a reference.[18] We now use it to fully understand mode construction in DLSPPW.

II. FIGURE OF MERIT AND CONFINEMENT FACTOR OF DLSPPW

Figure 1 schematically describes the DLSPPW geometry considered in the following. A dielectric ridge of thickness t and width w is deposited on a gold film of thickness d covering a glass substrate. For the calculations, the gold thickness and the incident wavelength are fixed to $d=50$ nm and $\lambda_0=780$ nm [$n_{Au}=0.18+i4.92$ (Ref. 19)], respectively. To evaluate the performance of a waveguide we introduce a set of parameters that can be optimized. These parameters are the confinement factor R, the mode area A_e (Ref. 14), and its

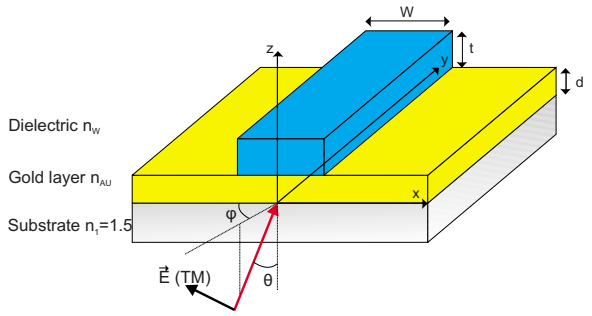

FIG. 1. (Color online) DLSPPW configuration. The guided mode is excited by a TM-polarized wave incident in total internal reflection.

propagation length L_{SPP}. In this section we systematically study the influence of the ridge thickness and width on these parameters.

Recently, Berini[14] proposed the concept of figures of merit for determining optimized dimensions of surface plasmon polariton waveguides. For SPP waveguides consisting of metal stripes, small sizes and limited losses are prerequisites. The figure of merit for these parameters can be defined as[14,20]

$$M_1^{2D} = \sqrt{\frac{\pi}{A_e}}(2 \times L_{SPP}). \tag{1}$$

Adapted for propagation length and mode area, this figure of merit lacks information on the mode confinement which is of great importance for applications in active plasmonics. If the dielectric layer is doped to introduce an external control of the guided SPP mode, the amount of mode sustained inside the dielectric stripe determines how strong the influence of the changes would be in the whole mode. The confinement factor measures the proportion of the mode energy inside the waveguide. A high degree of confinement would ensure a stronger interaction between the SPPs and an active material. We compute the confinement factor R as

$$R = \frac{\int\int_{\text{guide}} \vec{P} \cdot d\vec{S}}{\int_{-\infty}^{+\infty}\int_{z>0} \vec{P} \cdot d\vec{S}}, \tag{2}$$

where $\vec{P}$ is the poynting vector. Note that in the regime of thin-metal film ($d<60$ nm), the modes studied here are intrinsically leaky through the substrate. Consequently, we limit the integration above the substrate for the normalization.

Considering the application range of dielectric-loaded SPP waveguides, we have evaluated their performance based on both the figure of merit and the confinement factor. The mode properties are calculated using the effective index model (EIM) (Refs. 10 and 21) and the differential method.[18,22] In general an excellent agreement between the effective index model and the differential method is found except for the propagation length which is often overestimated in the EIM. This discrepancy is attributed to the limitation of the EIM in taking into account the corners of the dielectric stripe, which therefore disregards the mode scattering along these corners. Therefore, the DLSPPW properties accessible from the effective index model (number of modes, effective index values, cut-off conditions, mode expansion, and confinement) are determined first. The intensity distribution of the modes is then calculated using the differential method which is more time consuming compared to EIM.

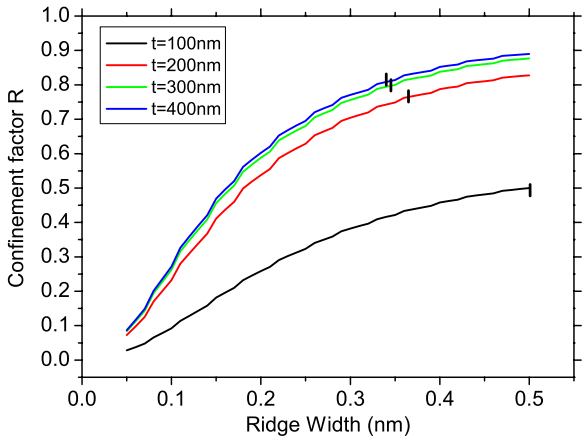

FIG. 2. (Color online) Confinement factor calculated using EIM for several PMMA film thicknesses as a function of ridge width. The crosses indicate the TM_{01} cut-off width. The PMMA optical index is $n_w=1.49$.

A. Thick dielectric load

We first consider the case of a thick dielectric load, i.e., with a thickness around $\lambda/2n_w=260$ nm. The dielectric stripe consists of poly-methyl-methacrylate (PMMA) since it is an electron-sensitive resist that can be structured by electron-beam (e-beam) lithography and it can be readily doped with different active substances. Using the effective index model, as described in detail in Ref. 10, we determine the confinement [Eq. (2)] of the mode supported by the DLSPPW. The values for the mode confinement as a function of the width of ridge w and for different PMMA thicknesses t are presented in Fig. 2. The field confinement increases with PMMA thicknesses and tends to saturate for thicknesses larger than 300 nm. Moreover, increasing the dielectric ridge width allows the excitation of higher-order modes in the waveguide.[10] In order to maximize the interaction between the mode and the polymer, we impose monomodal conditions, corresponding to ridge widths below 350 nm. Finally, a set of parameters (t,w) that combines good confinement and monomodal waveguide is around $t=350$ nm and $w=300$ nm.

Having determined an optimized set of parameters for the PMMA ridge, we investigate the mode characteristics using the differential method.[18,22] A detailed description of the differential method applied to DLSPPW analysis has been published elsewhere.[23]

Following the discussion above, we realized a sample with the following parameters (see Sec. III A): the gold film thickness is $d=50$ nm, the PMMA ridge width $w=240$ nm,

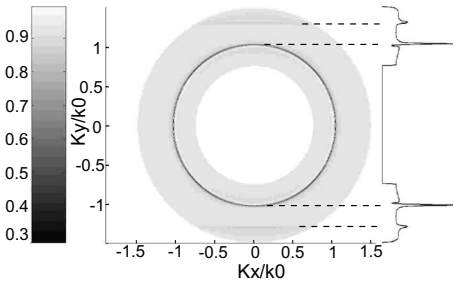

FIG. 3. Reflectivity map with varied incident angles θ and φ (see Fig. 1). The DLSPPW is made of a PMMA ridge of width $w=240$ nm and thickness $t=330$ nm. The incident wave-vector components along the x and y axes are $k_x/k_0=n_1 \sin\theta\cos\varphi$ and $k_y/k_0=n_1 \sin\theta \sin\varphi$, respectively.

and thickness $t=330$ nm. The incident wavelength is $\lambda=780$ nm. Note that by using the differential method, we obtain a mode propagation length in the range of $L_{SPP}=6.5\pm0.5$ μm for a ridge width varying from 150 to 500 nm. This justifies *a posteriori* that we only focused on the confinement properties when optimizing the ridge dimensions.

Figure 3 shows the reflectivity diagram calculated with the differential method when the DLSPPW is illuminated with a plane wave from below the substrate at different angles of incidence.[18] A low reflectivity circle is clearly visible at $n_{eff}=k_{\|}/k_0=1.02$ where $k_{\|}=(k_x^2+k_y^2)^{1/2}$ is the wave-vector component parallel to the gold surface. This is the signature of the excitation of the Au/air surface plasmon polariton mode. Two absorption lines also appear at $n_{eff}=|k_y/k_0|=1.30$. These two bands originate from light coupling to DLSPPW modes which propagates toward increasing y direction ($k_y/k_0>0$) or decreasing y direction ($k_y/k_0<0$) inside the guide.[18] Note that the same value for the effective index of the mode ($n_{eff}=1.30$) is obtained using effective index model.

Figures 4(a) and 4(b) show the electric-field intensity distribution of the mode across a section of the waveguide and its evolution along the propagation direction, respectively. The profiles are calculated using a TM-polarized incident beam oriented along the waveguide ($\varphi=90°$) and matched to the mode momentum [$\theta=\arcsin(n_{eff}/n_1)=60°$]. The calculations show that the mode is well confined by the dielectric structure and has its maximum at the Au/PMMA interface as expected from a SPP wave. The decay along the propagation is exponential. We deduce from Fig. 4(a) the confinement factor $R=69\%$ and from Fig. 4(b) a propagation length at $1/e$ attenuation of $L_{SPP}=6.1$ μm. R is in excellent agreement with the confinement calculated using the effective index model (see Fig. 2).

B. Thin dielectric load

While optimized mode confinement can be achieved by nearly squared waveguide sections (e.g., $w=350$ nm$\times t=300$ nm), DLSPPWs formed by thinner loads offer a different range of guiding properties.[15] In this section, we focus our attention on a 70-nm-thick dielectric. For this range of

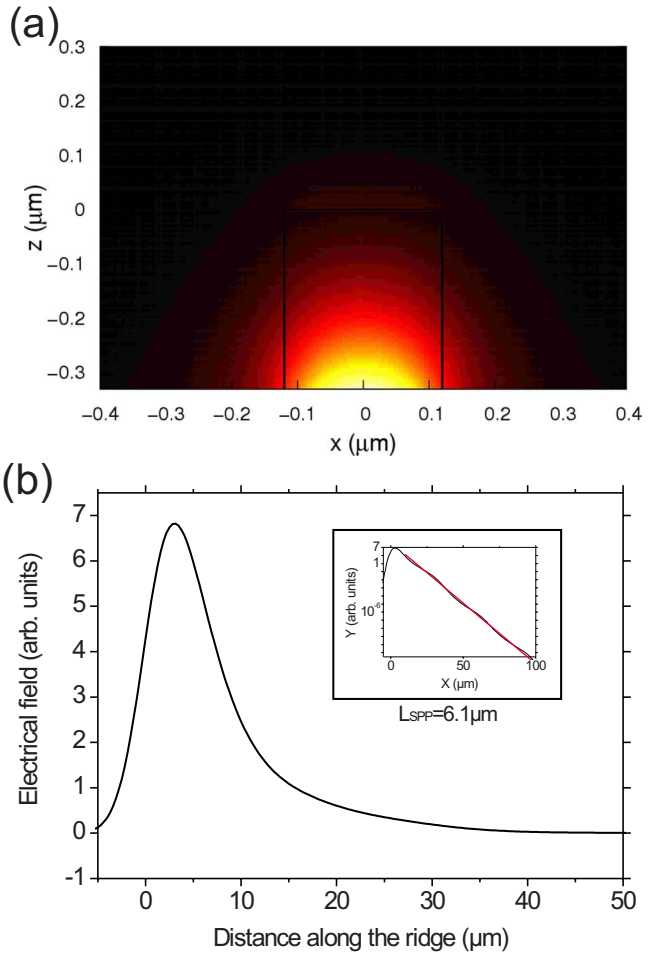

FIG. 4. (Color online) (a) Electrical-field intensity distribution inside the guide. The mode is excited using an incident wave at $\theta=60°$. (b) Cross section along the ridge center. The inset shows a linear fit in semilogarithmic scale.

thickness, the confinement R is small (see Fig. 2) and the mode substantially extends out of the dielectric structure. Nonetheless, these types of waveguides benefit from longer propagation length as compared with thick dielectric. Thin DLSPPW can therefore provide the basic units for designing more complex SPP routing (mode couplers, filters, etc.). In this respect, the figure of merit M_1^{2D} defined in Eq. (1) is the critical parameter.

On the basis of the effective index model, we first determine the modes supported by a 70 nm thin SiO_2 DLSPPW. The choice of SiO_2 over PMMA is dictated by its compatibility with current microelectronic technology (of interest if this kind of DLSPPW is useful in SPP routing systems) and do not change the general conclusions drawn so far.

Figure 5 shows the effective indices for the different TM modes supported by the DLSPPW. The effective index of the fundamental mode TM_{00} increases with w from the Au/air effective index ($n_{eff}=1.02$) up to that of a $Au/SiO_2(70\ nm)/air$ system ($n_{eff}=1.15$). Higher-order modes are populated when the ridge width increases. As an example, the TM_{01} and TM_{02} modes have a cut-off width at, respectively, 700 nm and 1.5 μm.

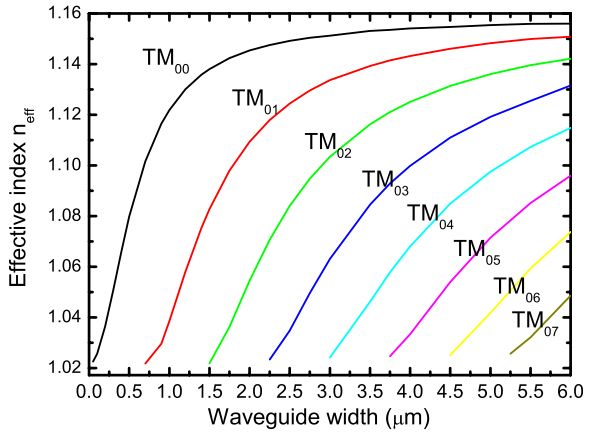

FIG. 5. (Color online) Effective indices of the fundamental and higher-order modes associated with a 70-nm-SiO_2 (n_w=1.453) DLSPPW as a function of the waveguide's width.

Figure 6 shows the calculated mode intensity pattern across the DLSPPW for several ridge widths. For very narrow waveguides only the fundamental mode TM_{00} is present. For the narrowest waveguide shown w=100 nm, the field intensity is spread across the dielectric loading (indicated by a blue rectangle in the figure) and the surrounding air media. Thus, the n_{eff} of the guided mode is comparable to that of the gold-air SPP mode. As the waveguide width increases, the TM_{00} mode becomes more confined in the SiO_2 loading as well as above the structure [see Figs. 6(b)–6(d)] and its effective index increases accordingly. Note that the dielectric load thickness is below TE_0 mode cutoff so that no TE-polarized mode is supported.[10]

It can be seen in Fig. 5 that the 70 nm SiO_2 DLSPPW becomes multimodal for a width larger than 700 nm. Note that the first higher-order appearing mode TM_{01} shows an odd field distribution (not shown here) and therefore cannot be excited by a plane wave impinging along the waveguide direction. On the contrary, even modes can be easily excited and their corresponding field patterns for a width w=4 μm are shown in Figs. 6(e) and 6(f).

Figure 7 represents the figure of merit M_1^{2D} associated to the fundamental mode TM_{00} calculated from Eq. (1) using

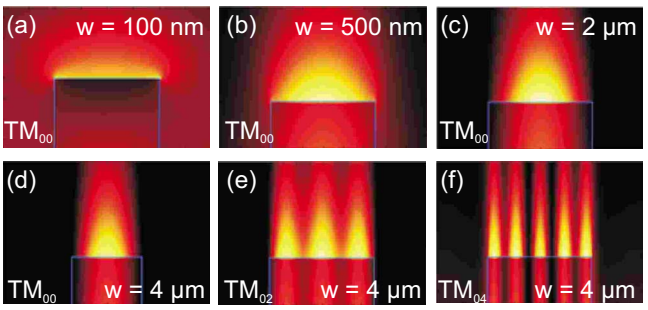

FIG. 6. (Color online) Calculated mode intensity distribution across the DLSPPW in the air half space. [(a)–(c)] TM_{00} patterns for waveguide widths w=0.1, 0.5, and 2 μm, respectively. The dielectric waveguide is indicated by the blue rectangle. [(d)–(f)] Pattern for the even modes TM_{00}, TM_{02}, and TM_{04} for a waveguide of w=4 μm. The aspect ratios are different for the sake of visibility.

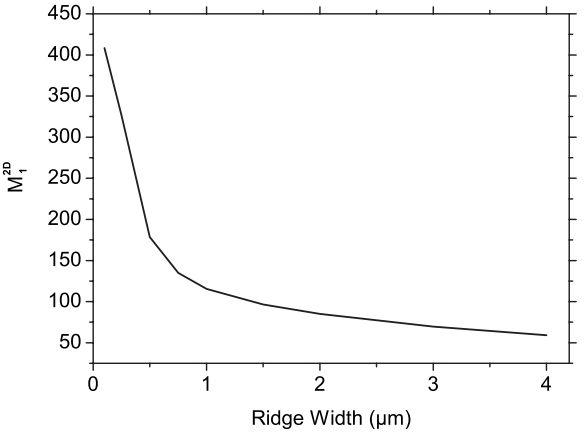

FIG. 7. Figure of merit obtained from differential method for the fundamental TM_{00} mode for a 70-nm-thin SiO_2 ridge loaded on a 62-nm-gold film.

the differential method. Thin ridges are characterized by a better figure of merit than thick ones (not shown). In spite of the spreading of the mode outside the dielectric ridge, the longer propagation distances of the mode in this case lead to a large value for M_1^{2D}; mainly for narrow waveguides. Note also that the values of the M_1^{2D} obtained for the thin SiO_2 DLSPPW are high despite the large ohmic losses of gold at the frequency we consider.[20]

III. EXPERIMENTS

A. Thick dielectric load

With the aim of controlling the numerical results, a sample was prepared according to the following procedure: a gold layer with a thickness of 50 nm was first evaporated on a glass substrate. A 330-nm-thick electron-sensitive PMMA layer was then spin coated onto the gold film. The PMMA was then exposed by standard *e*-beam lithography to form a ridge of 240 nm width. The surface plasmon modes supported by the waveguide can be excited following different diascopic or episcopic excitation schemes. A schematic of the setup in diascopic configuration is shown in Fig. 8. A 0.52 numerical aperture (NA) objective incident from the air side focuses a collimated laser beam onto the ridge structure. The polarization state was controlled by inserting a retarder in the optical path. Momentum transfer through scattering on the ridge or on a defect ensured that part of the incident energy was coupled in the SPP mode. To investigate the characteristics of the guided modes, we collected the intrinsic radiation leaking through the gold film by using a high numerical aperture oil immersion objective (Nikon 60× and NA=1.49). The intensity of the leakage radiation emitted at the substrate/gold interface is directly related to the intensity distribution of the SPP mode and provides therefore a unique mean to easily assess SPP properties.

1. Measurement at λ_0=780 nm

A typical DLSPPW structure of the sample is shown in the bright-field optical micrograph of Fig. 9(a). A defect,

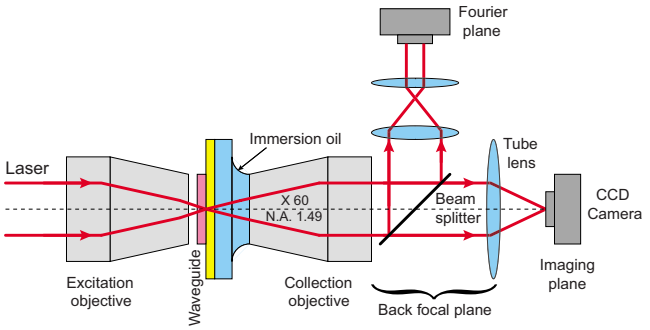

FIG. 8. (Color online) Sketch of the leakage radiation microscopy setup. A 0.52 NA objective focuses the incident light onto the structure or a defect. The modes are excited through scattering and momentum transfer. Leakage radiation of the guided modes is collected with a 1.49 NA objective and recorded either in the image plane or in the Fourier plane.

helping to convert part of the incident energy into the SPP mode, is indicated by the white circle. Figure 9(b) shows the spatial intensity distribution of the radiation leakage as recorded in the image plane. The focalization of the incident light by the 0.52 objective is readily visible in the bottom part of the image as a bright overexposed spot. The SPP guided mode is recognized as the confined streak of light propagating from the bottom to the top of the image. An exponential fit of the decaying intensity gives a propagation length of 5.5 μm, in very good agreement with the calculated value [6.1 μm; see Fig. 4(b)].

Figure 9(c) shows the leakage radiation recorded in the Fourier plane of the microscope. The bright central disk corresponds to the numerical aperture (NA=0.52) of the top illuminating objective and is used for calibration of the Fourier plane.[18] The two symmetric half moons that appear at $n_{\mathrm{eff}}=1.02\pm0.03$ correspond to leakage radiation coming from the Au/air SPP mode. The NA of the objective limits the upper value of the mode index, which is 1.49 in our

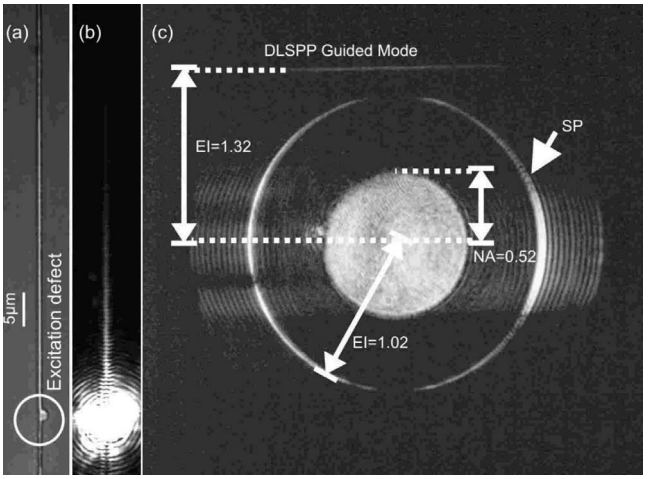

FIG. 9. (a) Optical micrograph of a typical PMMA waveguide fabricated on a gold substrate. The DLSPPW modes are excited by focusing a TM-polarized beam on the defect marked in (a). LRM observation of the propagation along the waveguide: in the (b) image plane and in the (c) Fourier plane.

TABLE I. Experimental and theoretical values (calculated using differential method and effective index model) of the mode effective index.

Effective index			
λ_0 (nm)	Differential method	EIM	Experiment
750	1.32	1.31	1.28
760	1.32	1.31	1.28
770	1.31	1.30	1.26
780	1.30	1.30	1.26
790	1.29	1.29	1.26
800	1.28	1.28	1.26
810	1.28	1.28	1.25
820	1.27	1.27	1.24
830	1.26	1.27	1.24
840	1.26	1.26	1.23
850	1.25	1.26	1.23
860	1.24	1.26	NA
870	1.24	1.25	NA
880	1.23	1.25	NA
890	1.23	1.24	NA
900	1.22	1.24	NA

experiment. The signature of the guided mode inside the DLSPPW appears as a horizontal line in the Fourier plane. This line corresponds to the value of the propagation constant and has a measured effective index of $n_{\mathrm{eff}}=1.32\pm0.04$, in fair agreement with the theoretical reflectivity measurement shown in Fig. 3. Note however that only the mode that propagates in the forward direction appears in Fig. 9(c) because the waveguide is not well defined below the defect used for the excitation. Additionally, the intensity of the DLSPP mode is significantly weaker than the other features on Fig. 9(c) because of the SPPs coupling efficiency of our excitation scheme.

2. Measurements at different wavelengths

Wavelength influence on the mode properties is now considered. Table I and Fig. 10 present the effective indices and propagation lengths measured and calculated for 750 nm $\leq\lambda_0\leq$900 nm. Despite a few atypical points, the L_{SPP} evolution is quite monotonous with increasing wavelength since the imaginary part of the gold refractive index decreases in the infrared domain. A fair agreement is obtained between experimental data and numerical simulations. Note that effective indices for $\lambda_0\geq860$ nm were not measured experimentally since low radiative losses at these wavelengths lead to poor signal-to-noise ratios in the LRM images.

B. Thin dielectric load

The fabrication procedure for thin SiO_2 loads also relies on standard *e*-beam lithography followed by thermal deposition of SiO_2 layer and a liftoff of the resist. Thin DLSPPWs were also characterized by leakage radiation microscopy.

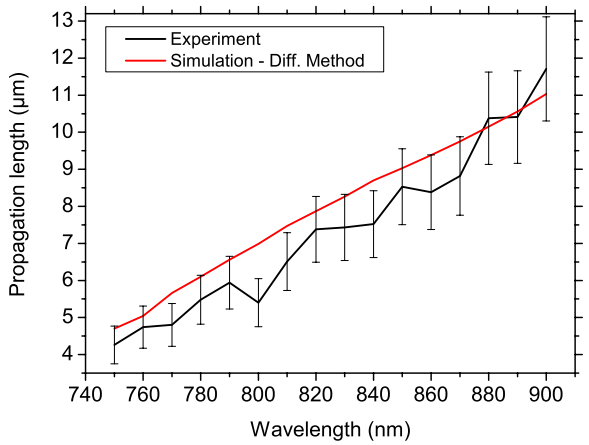

FIG. 10. (Color online) Experimental and theoretical values (calculated using differential method) of the propagation length as a function of the wavelength for a 330 nm × 240 nm PMMA DLSPPW.

Figure 11 shows the experimental images for thin waveguides with several ridge widths. Instead of exciting the DLSPPW mode by focusing onto a defect,[24] SPPs on the bare 62-nm-thick Au film were excited using a total internal reflection (TIR) illumination scheme.[15,25] Therefore, the incident TM-polarized light having a wavelength $\lambda_0=800$ nm was displaced from the optical axis and slightly focused onto the back focal plane of the immersion-oil objective (Olympus 60× and NA=1.45). This results in illuminated areas of 10 μm by 15 μm that appear as white distorted ellipses in Figs. 11(b)–11(e). The back-reflected field saturates the charge-coupled device (CCD) camera. We focus the beam several microns before the entrance of the dielectric stripe, as sketched in Fig. 11(a). The light matching k_{SPP} excites the SPPs having most of its energy at the gold/air interface. The SPPs propagate a few tens of micrometers toward the DLSPPW as indicated by the red arrow. During propagation, the SPPs produce the leakage radiation visible in Figs. 11(b)–11(e) in between the incidence spot and the dielectric stripe. The modes existing in the DLSPPW are leaky because of the finite gold layer thickness of 62 nm and can be easily imaged by LRM.

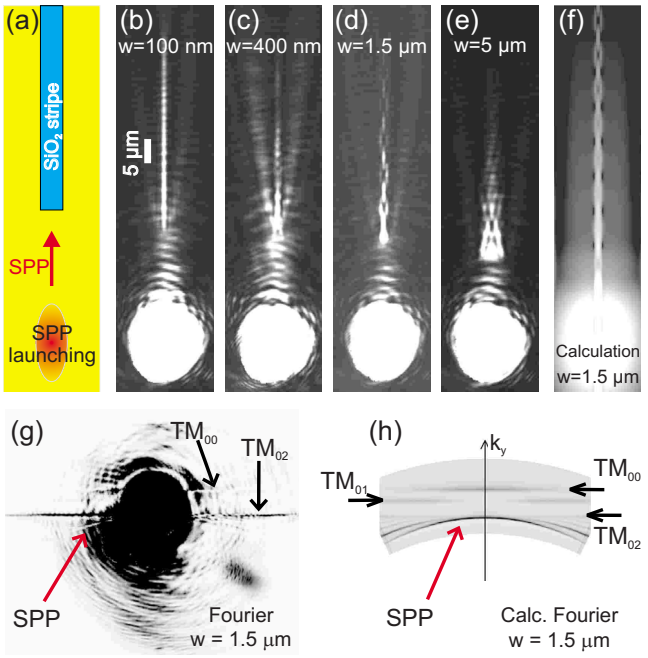

FIG. 11. (Color online) LRM images of light propagating through a thin SiO_2 ridge (t=70 nm) waveguide for different widths w at $\lambda_0=800$ nm. (a) Sketch of the excitation configuration. The SPPs are launched on the gold film by TIR illumination and hit the end face of the DLSPPW, thereby exciting the waveguide modes. [(b)–(e)] Direct-space LRM images of the waveguides. (f) Calculated (differential method) field intensity for light propagating along a DLSPPW of width 1.5 μm excited by a Gaussian beam impinging on the waveguide. (g) Fourier plane image corresponding to the waveguide of $w=1.5$ μm. (h) Calculated reflectivity map in a portion of the reciprocal space for a waveguide of $w=1.5$ μm. The excited modes are indicated by arrows in the image.

The LRM images for DLSPPW of different widths are displayed in Figs. 11(b)–11(e). The images clearly reveal the strong dependence of the mode characteristics on the width of the dielectric loading. For a 5-μm-wide SiO_2 stripe [Fig. 11(e)], which has nearly the same width as the incident SPPs, most of the SPPs are converted into the DLSPPW modes. The intensity along the waveguide decays much more rapidly compared to SPPs on the unloaded gold-air interface. For narrower DLSPPWs, the section of the DLSPPW does not fully overlap the width of the incident SPPs and three distinct regions can be distinguished. The first one corresponds to leakage radiation along the waveguide and originates from the coupling of the incident SPPs into the guiding structure. The second region corresponds to the portion of the incident SPPs not coupled into the waveguide. This uncoupled part propagates sidewise the guides along both edges and is readily visible in Figs. 11(b)–11(d). Finally, the third region is associated with incident SPP which is backreflected and/or scattered by the DLSPPW edge. This latter portion is dominantly emitted into the air space.

From the LRM images, we can determine the characteristic properties of the waveguides, namely, the effective refractive index n_{eff} and the propagation length L_{SPP}. The latter was determined by fitting the intensity decay along the waveguides for a variety of widths and is displayed in Fig. 12. In the case of a multimodal waveguide, the measured L_{SPP} represents an average decay length considering all the excited modes.

The upper limit for L_{SPP} is given by the unloaded gold surface and is indicated by the horizontal red dashed line in Fig. 12 (theory $L_{SPP}=35.3$ μm). The experimentally determined decay value for our gold films is $L_{SPP}=33.6$ μm, in very good agreement with this theoretical value. The green dashed line at $L_{SPP}=9$ μm corresponds to a complete 70-nm-SiO_2 dielectric film and provides a lower bound for L_{SPP}. This lower limit is reached for DLSPPW width greater than approximately 2 μm. For narrower waveguides, the value of L_{SPP} increases significantly toward the upper limit. This general behavior is in good agreement with the figure of merit M_1^{2D} shown in Fig. 7: for narrow waveguides M_1^{2D} strongly increases as a consequence of the higher propagation length.

The experimental effective indices of the DLSPPW modes inside the waveguides were assessed from LRM Fou-

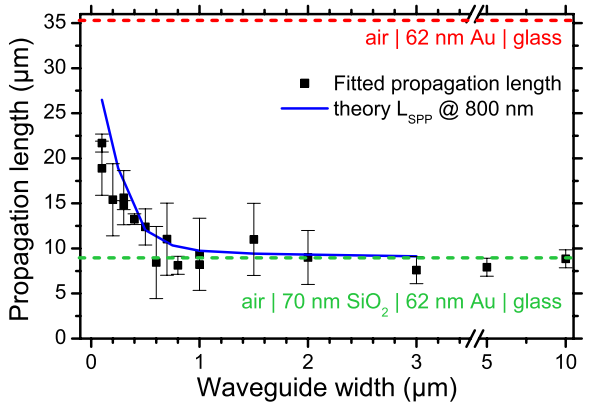

FIG. 12. (Color online) Evolution of the propagation length L_{SPP} with the width w of a thin SiO_2 ridge (t=70 nm) waveguide (TM polarization and λ_0=800 nm). The red and green dashed lines correspond to the upper and lower limits of this propagation length, respectively: the plasmon of the interface air/Au and that of the interface air/70-nm-SiO_2/Au. The blue line shows the theoretical values for L_{SPP}, corresponding to TM_{00} mode only, calculated with the differential method.

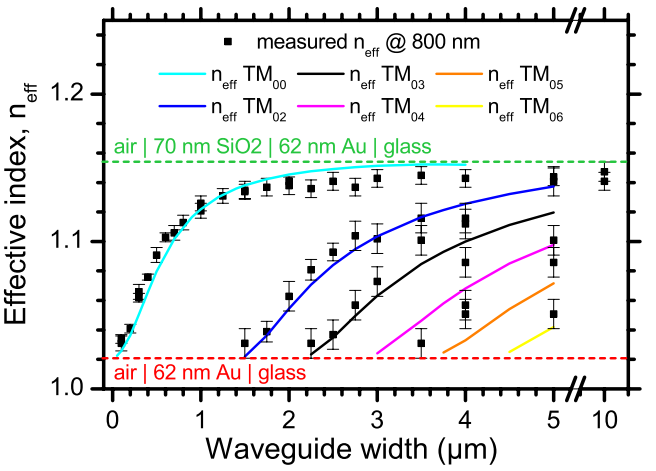

FIG. 13. (Color online) Evolution of the mode effective index n_{eff} with the width w of a thin SiO_2 ridge (t=70 nm) waveguide (TM polarization and λ_0=800 nm). The values of n_{eff} should be comprised within those of the plasmon in an air/Au interface (red dashed line) and the plasmon in an air/70-nm-SiO_2/Au interface (green dashed line). The solid lines report the effective index obtained from EIM (see Fig. 5).

rier images, as the one shown in Fig. 11(g). In contrast to Fig. 9(c) where the waveguided mode was excited by the use of a local defect, here the TIR configuration outlined above was used. Figure 11(g) is the Fourier plane image of a DLSPPW with w=1.5 μm [Fig. 11(d)]. The excitation geometry gives rise to a strong reflection spot in the Fourier image. The size of the spot is a measure of the distribution of incident wave vectors. To efficiently couple the SPPs, the location of the spot in the reciprocal space is adjusted to coincide with the SPP resonant wave vectors. The coupling to the SPP mode is detected by the presence of a dip within the distribution. This dip is however not clearly visible in the image since the saturation of the detector was adjusted to enhance the weak signature of the waveguided modes. Note that outside the incident distribution of wave vectors, the SPP coupling at the Au/air interface can be recognized as a small crescent (indicated with an arrow in the figure). It originates from SPPs propagating in directions diverging from the incident excitation. More importantly, the signature of the DLSPPW modes also marked with arrows appears as straight bright lines extending out of the incident wavevector distribution. For this particular width, two modes are observed in the Fourier plane image of Fig. 11(g). The n_{eff} of the various modes appearing for each waveguide was measured using the k_{SPP} position of SPPs propagating at the bare gold/air interface as a reference. The results are gathered in Fig. 13.

As expected, the effective indices of the DLSPPW modes are within the limits given by the bare gold surface (n_{eff} =1.02, dashed red line) and a gold surface completely loaded with 70 nm SiO_2 (n_{eff}=1.15, dashed green line). In order to identify the order of the modes associated for each value, we have also plotted the n_{eff} values obtained from the EIM calculations presented in Fig. 5. The experimental results for n_{eff} are in good agreement with the predictions and the small differences originate from experimental uncertainties such as the exact shape of the dielectric loading, the surface roughness, and the exact thickness of the SiO_2 layer. For instance, a thickness difference of only 5 nm would shift the upper limit of n_{eff} from 1.154 (70 nm SiO_2) to 1.14 (65 nm SiO_2). We note that the TM_{01} mode was not observed for any of the waveguides, while higher-order modes were detected. This particular mode has an odd symmetry of the field and cannot be excited with a beam impinging along the waveguide direction. This explanation is confirmed by the calculated reflectivity map shown in Fig. 11(h), corresponding to a DLSPPW of w=1.5 μm. For this width, three modes are supported: TM_{00}, TM_{01}, and TM_{02}. However, only TM_{00} and TM_{02} are intersecting with k_x=0 value, indicating that they can be excited by a beam parallel to the waveguide. The TM_{01} mode has a signature for $k_x \neq 0$ values and can only be excited with a tilted illumination. The absence of the TM_{01} mode in our experiment indicates that the angular spreading of the beam used to excite the waveguides was not broad enough to excite this mode.

The multimode nature of the DLSPPWs for w greater than approximately 1.5 μm does not only manifest itself in the Fourier plane but in the LRM images of Figs. 11(b)–11(e). The two wider waveguides w=1.5 and 5 μm are certainly multimode and they show modulated intensity patterns. The difference in the intensity distribution inside the waveguides indicates that different modal structures are involved. The 1.5-μm-wide waveguide, for instance, presents two identified modes: TM_{00} and TM_{02}. The field distribution of these two modes shown in Fig. 6 has, respectively, one central maximum and three maxima. The interference between these two modes creates a beating with a chainlike distribution observed in Fig. 11(d). The beating period of the intensity along the center of this waveguide Δ, as calculated from the image, is 7 ± 0.2 μm. Beating of the two considered modes TM_{00} and TM_{02} can be obtained from the expression $\Delta = 2\pi/(k_{TM_{00}} - k_{TM_{02}}) = 6.9$ μm, in good agreement with the measured value. Figure 11(f) shows the field intensity distri-

bution along a 1.5 μm wide DLSPPW calculated with the differential method and excited by a Gaussian beam. The angular spread of the Gaussian beam was restricted to only excite the TM_{00} and TM_{02} modes. The intensity distribution shows a very similar chainlike pattern as observed in the experimental image.

For waveguides being narrower than $w < 1.5$ μm, only the fundamental mode is excited and the intensity shows no spatial pattern across the waveguide [see Figs. 11(b) and 11(c)]. We have however detected some beating in the intensity along these waveguides whose periodicity is given by $\Delta = 2\pi/(k_{TM_{00}} - k_{SPP})$. This beating comes from the interference of the fundamental DLSPPW mode and SPPs propagating on the gold film. Hence, the beating period increases for narrower DLSPPW and, for example, cannot be measured for the 100-nm-wide waveguide.

In summary, since the incident SPPs at the gold/air interface couple simultaneously to all of the available guided modes, the propagation distance and intensity distribution of thin DLSPPW become strongly dependent of w. For $w \geq 1.5$ μm, multiple modes are excited generating a strong beating and L_{SPP} is very close to the SPP decay of a homogeneous gold/SiO_2 interface (about 9 μm). This reflects the fact that the excited modes are mostly confined laterally within the silica load in this case. When reducing w below 1.5 μm, the incident energy couples to the TM_{00} mode only. For very narrow DLSPPW, the field extends further into the air resulting in an increase in the propagation length and lower effective index of the mode. Despite low transversal confinement, the figure of merit M_1^{2D} shows a respectable value (see Fig. 7) and efficient guiding is indeed achieved along 100-nm-wide DLSPPW with $L_{SPP} = 20$ μm.

IV. CONCLUSION AND PERSPECTIVE

In this paper, dielectric-loaded surface plasmon polaritons waveguides were theoretically and experimentally investigated by leakage radiation microscopy in direct and Fourier planes. Depending on the thickness of the dielectric load, the figure of merit or mode confinement can be optimized. For a thin load, the large values of the figure of merit allow the propagation of surface plasmon guided modes over distances of several tenths of micrometer in the near-infrared region. For thicker loads, the decay is shorter but the three-dimensional confinement is drastically increased. This regime of thickness is suitable for applications requiring a large density of plasmonic devices. The calculated values of the effective indices and decay lengths of the guided modes obtained with our numerical approach are in agreement with the experimental values. This is encouraging for extending the range of our calculation to telecom bands ($\lambda_0 = 1300$ nm or 1550 nm). Note that at these wavelengths, leakage radiation microscopy is probably not a suitable tool. Radiation losses through the metal are negligible and near field microscopy is more appropriate.[26–28]

ACKNOWLEDGMENTS

The authors gratefully acknowledge T. Holmgaard and S. I. Bozhevolnyi for fruitful discussions. This work was supported by the European Commission through the PLASMOCOM project (under Project No. EC FP6 IST 034754 STREP). M.U.G thanks the Spanish Ministry of Education for funding under the "Ramón y Cajal" program.

*jonathan.grandidier@u-bourgogne.fr
†Also at ICREA-Institució Catalana de Recerca i Estudis Avançats, Barcelona, Spain.

[1] W. Barnes, A. Dereux, and T. Ebbesen, Nature (London) **424**, 824 (2003).
[2] E. Ozbay, Science **311**, 189 (2006).
[3] R. Charbonneau, P. Berini, E. Berolo, and E. Lisicka-Shrzek, Opt. Lett. **25**, 844 (2000).
[4] J. C. Weeber, Y. Lacroute, and A. Dereux, Phys. Rev. B **68**, 115401 (2003).
[5] S. I. Bozhevolnyi, V. S. Volkov, E. Devaux, J. Y. Laluet, and T. W. Ebbesen, Nature (London) **440**, 508 (2006).
[6] E. Moreno, S. G. Rodrigo, S. I. Bozhevolnyi, L. Martín-Moreno, and F. J. García-Vidal, Phys. Rev. Lett. **100**, 023901 (2008).
[7] J. A. Dionne, H. J. Lezec, and H. A. Atwater, Nano Lett. **6**, 1928 (2006).
[8] P. Ginzburg and M. Orenstein, Opt. Express **15**, 6762 (2007).
[9] B. Steinberger, A. Hohenau, H. Ditlbacher, A. L. Stepanov, A. Drezet, F. R. Aussenegg, A. Leitner, and J. R. Krenn, Appl. Phys. Lett. **88**, 094104 (2006).
[10] T. Holmgaard and S. I. Bozhevolnyi, Phys. Rev. B **75**, 245405 (2007).
[11] A. V. Krasavin and A. V. Zayats, Appl. Phys. Lett. **90**, 211101 (2007).
[12] B. Steinberger, A. Hohenau, H. Ditlbacher, F. R. Aussenegg, A. Leitner, and J. R. Krenn, Appl. Phys. Lett. **91**, 081111 (2007).
[13] T. Holmgaard, Z. Chen, S. I. Bozhevolnyi, L. Markey, A. Dereux, A. V. Krasavin, and A. V. Zayats, Opt. Express **16**, 13585 (2008).
[14] P. Berini, Opt. Express **14**, 13030 (2006).
[15] A. Hohenau, J. Krenn, A. Stepanov, A. Drezet, H. Ditlbacher, B. Steinberger, A. Leitner, and F. Aussenegg, Opt. Lett. **30**, 893 (2005).
[16] B. Hecht, H. Bielefeldt, L. Novotny, Y. Inouye, and D. W. Pohl, Phys. Rev. Lett. **77**, 1889 (1996).
[17] A. Bouhelier, T. Huser, H. Tamaru, H.-J. Güntherodt, D. W. Pohl, F. I. Baida, and D. Van Labeke, Phys. Rev. B **63**, 155404 (2001).
[18] S. Massenot, J. Grandidier, and A. Bouhelier, G. Colas des Francs, J. -C. Weeber, L. Markey, A. Dereux, J. Renger, M. U. González, and R. Quidant, Appl. Phys. Lett. **91**, 243102 (2007).
[19] *Handbook of Optical Constants of Solids*, edited by E. D. Palik (Academic, San Diego, 1985).
[20] R. Buckley and P. Berini, Opt. Express **15**, 12174 (2007).
[21] D. Marcuse, *Theory of Dielectric Optical Waveguides* (Academic, New York, 1991).

[22] M. Nevière and E. Popov, *Light Propagation in Periodic Media, Differential Theory and Design* (Marcel Dekker, New York, 2003).
[23] S. Massenot, J.-C. Weeber, and A. Bouhelier, G. Colas des Francs, J. Grandidier, L. Markey, and A. Dereux, Opt. Express **16**, 17599 (2008).
[24] J. Renger, S. Grafström, and L.-M. Eng, Phys. Rev. B **76**, 045431 (2007).
[25] A. Bouhelier and G. P. Wiederrecht, Opt. Lett. **30**, 884 (2005).
[26] P. Dawson, F. de Fornel, and J.-P. Goudonnet, Phys. Rev. Lett. **72**, 2927 (1994).
[27] S. I. Bozhevolnyi, V. S. Volkov, E. Devaux, J.-Y. Laluet, and T. W. Ebbesen, Nature (London) **440**, 508 (2006).
[28] T. Holmgaard, S. I. Bozhevolnyi, L. Markey, and A. Dereux, Appl. Phys. Lett. **92**, 011124 (2008).